



# Stretch-orientation-induced reduction of friction in well-entangled bidisperse blends: a dual slip-link simulation study

Souta Miyamoto<sup>1</sup> · Takeshi Sato<sup>2</sup> · Takashi Taniguchi<sup>1</sup>

Received: 28 June 2022 / Revised: 2 November 2022 / Accepted: 3 November 2022 / Published online: 15 December 2022  
© The Author(s) 2022

## Abstract

We investigated the rheological properties of bidisperse entangled-polymer blends under high-deformation-rate flows by slip-link simulations with a friction reduction mechanism. The friction reduction mechanism induced by the stretch and orientation (SORF) is important to predict the viscoelasticity under uniaxial elongational flows. To test the applicability of this mechanism for bidisperse systems, we incorporated an expression of friction reduction (Yaoita et al. *Macromolecules* 45:2773–2782 2012) into the Doi-Takimoto slip-link model (DT model) (Doi and Takimoto *Philos Trans R Soc Lond A* 361:641–652 2003). For six experimental bidisperse systems, i.e., four polystyrene blends and two polyisoprene blends, the extended DT model where the order parameter of the friction reduction mechanism is evaluated through the component averages succeeds in reproducing the data under uniaxial elongation and shear. This success is due to the suppression of the stretch of the longer chains using the statistical average over each component. Through this study, the SORF expression improves the rheological prediction for bidisperse entangled polymer melts under uniaxial elongational flows with strain rates comparable to or larger than the inverse of the Rouse relaxation time of the longer chains. Additionally, the predictions with the SORF using the component average for the stretches reproduce the steady viscosities because under elongational flows, the states of the components with different molecular weights clearly differ from each other depending on their Rouse relaxation time. The finding means that for chain dynamics, the friction coefficient is determined by the state of the surrounding polymer chains and the state of the chain.

**Keywords** Polymer melt · Entanglement · Slip-link · Bidisperse blends · Nonlinear viscoelasticity

## Introduction

The rheological properties of a polymer melt in an entangled state attract much attention due to their importance in polymer processing. In typical industrial conditions, a polymer melt with molecular weight distribution is used to tune rheological properties (Ferry 1980). Thus, it is

important to investigate the relation between the rheology and the compositions of the well-entangled polymeric system. For such a purpose, bidisperse polymer blends have been extensively studied as a first step to understand the rheology of polymer melts with arbitrary molecular weight distributions, as explained in detail below.

Experimental studies on the rheology of bidisperse polymer melts have been made for several decades (Mantia et al. 1986; Minegishi et al. 2001; Nielsen et al. 2006; van Ruymbeke et al. 2010; Hengeller et al. 2016). Linear rheology involves not only the superposition of the rheology of monodispersed systems but also contributions from coupled dynamics (Viovy et al. 1991). The elongational viscosity has been measured by the Meissner-type rheometer by Minegishi et al. (2001) and by the filament stretching rheometer by several groups (Nielsen et al. 2006; Hengeller et al. 2016). Among these studies, one of the interesting findings is that polymer blends containing a small amount of ultrahigh-molecular-weight polymers show significant strain hardenings under

✉ Takashi Taniguchi  
taniguch@cheme.kyoto-u.ac.jp

Souta Miyamoto  
s.miyamoto@cheme.kyoto-u.ac.jp

Takeshi Sato  
takeshis@scl.kyoto-u.ac.jp

<sup>1</sup> Department of Chemical Engineering, Graduate School of Engineering, Kyoto University, Kyoto 615-8510, Japan

<sup>2</sup> Institute for Chemical Research, Kyoto University, Kyoto 611-0011, Japan

elongational flows (Minegishi et al. 2001). Nielsen et al. (2006) examined polystyrene blends and found that the maximum steady-state elongational viscosity became indistinguishable from three times the zero-shear viscosity calculated from linear viscoelasticity as the concentration of higher-molecular-weight chains increased in their examined samples. Hengeller et al. (2016) classified the time regimes for the relaxations after cessation of elongational flow for the bidisperse system. The relaxations after cessation of the steady elongations exhibit the three regimes originating from the dynamics of short, long, or both short and long polymer chains. To predict the mechanical properties based on the coupled dynamics over the components, it is desirable to develop a coarse-grained model.

The theoretical and numerical models of polymers have rationalized the molecular-based mechanism and reproduced the rheological properties by considering the coupled dynamics among the polymer chains. The models for entangled polymer melts are based on the bead-spring model and the tube model (Doi and Edwards 1986). For entangled polymers, the pioneering model is the famous tube model. The important dynamics of the tube are reptation, the change in the tube length, and the release of entanglements. Based on the original tube model, slip-link models (Hua and Schieber 1998; Masubuchi et al. 2001; Doi and Takimoto 2003) and slip-spring model (Likhtman 2005) were developed to numerically predict the rheological properties (Masubuchi 2014). These models can quantitatively reproduce the rheological properties in the linear and near-linear response regimes. However, it is difficult to predict some phenomena under high deformation rate flows because of the lack of the mechanisms required to predict nonlinear rheology. For example, typical slip-link models cannot predict the decrease in the steady viscosities of entangled polymer melts with strain rates under uniaxial elongational flows (Doi and Takimoto 2003).

For the unexplained rheological behavior under high deformation rate flows, friction reduction between a segment and the surrounding polymers induced by the stretched and oriented polymers (SORF mechanism) has been proposed (Ianniruberto et al. 2012). For the rheology of entangled and unentangled polymer melts, some studies support that the SORF is important for accurate predictions of nonlinear rheology (Ianniruberto et al. 2020; Matsumiya and Watanabe 2021). For entangled systems, Masubuchi and coworkers extensively examined nonlinear rheological properties by the primitive chain network (PCN) model. After developing the PCN model with SORF for linear polystyrene (Yaoita et al. 2012), they examined the universality of SORF (Masubuchi et al. 2014a), and the associated predictions under biaxial elongational flows (Takeda et al. 2018) and planar elongational flows (Takeda et al. 2020). Moreover, they investigated the applicability for pom-pom

polymers (Masubuchi et al. 2014b) and for star polymers (Masubuchi et al. 2021). Subsequently, Sato and Taniguchi (2019) studied the SORF by extending the slip-link model developed by Doi and Takimoto (2003). Tests for unentangled polymer melts have also been reported with the dumbbell model (Watanabe et al. 2020) and the Rouse model (Sato et al. 2021). While the SORF mechanism has been tested for monodispersed polymers, few studies have examined the effect of such a mechanism in bidisperse melts.

With the PCN model, the SORF expression has been tested for three bidisperse samples containing small amounts of the high-molecular-weight polymers (Takeda et al. 2015). Takeda et al. (2015) examined the SORF expression proposed by Yaoita et al. (2012) with the PCN model. They found that the PCN model reproduces the rheology of the bidisperse well-entangled polystyrene melts reported by Nielsen et al. (2006) and that the SORF mechanism explains the data under high-strain-rate elongational flows. In their results, at elongational strain rates below the inverse of the Rouse relaxation time of the long-chain component, suppressing the stretches of the long chains improves the rheological predictions. On the other hand, at elongational strain rates above that, the relaxations of the short chains suppress the SORF effects. Note that two models, namely, the slip-spring model (Read et al. 2018) and the Rolie-double-Poly (RDP) model (Boudara et al. 2019), can predict the linear and nonlinear rheological properties well, but these works still do not adopt the SORF mechanism. This RDP model can predict the transient viscosities within the regime of a short time; on the other hand, the steady elongational viscosities have difficulty in predictions under high-deformation-rate flows. We have to clarify whether the SORF mechanism is generally effective by making assessments based on more evidence, e.g., systems consisting of a larger amount of high-molecular-weight polymers.

From the viewpoint that the friction of a chain with others is a many-body problem, the coupling of the state of the entangled chain itself with the environment has not been investigated in depth. Specifically, unlike a monodispersed system where the state of a chain is statistically the same as the states of the surrounding chains, in a bidisperse system, the state of a longer or shorter entangled chain itself and the state of environments that can be evaluated by averaging the surrounding polymer chains might be different. Thus, the following question arises regarding how the friction coefficient (tensor) is determined by the state of a considering chain and/or the state of the environment around it, which factor is more dominant, the state of the considering chain or the state of the environment. Judging from the fact that the nonlinear rheology of bidisperse polymer melts has not been well tested, we should also consider the comparison of the two contributions from the

considered chain and the environment in the extension to the bidisperse systems.

In this study, we assess the SORF mechanism for the bidisperse entangled polymer melts because the empirical relation used in the previous study (Takeda et al. 2015) has arbitrariness in using bidispersed polystyrene melts. In more detail, the SORF expressions thus far proposed are obtained from the monodisperse system; thus, the contribution originating from the difference in the states of the components has been ignored. This study takes into account the contribution to the friction reduction from the states of the long- and short-chain components. For such a purpose, we employ the pseudo-single-chain slip-link model, for which the effect of the SORF mechanism on the rheological properties has been tested in the case of monodisperse entangled polymer melts (Sato and Taniguchi 2019).

The contents of the present paper are as follows. In section “Model,” we explain the slip-link model and the SORF extension, and in section “Results and discussion,” we show the simulation results for six experimental samples. In section “Conclusions,” we summarize and discuss the results.

## Model

### Doi Takimoto original slip-link model

We employ a dual slip-link model developed by Doi and Takimoto (2003), namely, DT model. Here, “dual” refers to the assumption that an entanglement is made of two points on different chains. An entangled polymer chain is modeled by a primitive path, the two tails, and the slip-links on the path. The slip-links are pinned in space. A polymer molecule has two tails, and one-end of a tail is fixed by a slip-link and the other end is free. Each tail is considered to be an ideal chain. From the viewpoint of rheological properties, the entangled polymer chain is characterized by the number of entanglements at equilibrium  $Z_{eq}$  and the maximum stretch ratio  $\lambda_{max}$ . The units for the model are the length of a strand between two adjacent slip-links at equilibrium  $a$ , the Rouse relaxation time of a strand  $\tau_e$ , and a stress value  $\sigma_e$  connected to the plateau modulus.

The state of the  $i$ th polymer chain can be described by the positions of the slip-links  $\{\mathbf{R}\}$ , the length of the two tails  $\{s_{head}, s_{tail}\}$ , the numbers of entanglements of a chain  $Z$ , and the pair list of the slip-links. The primitive path length of the  $i$ th polymer chain  $L^i$  is calculated as

$$L^i = s_{head}^i + s_{tail}^i + \sum_{k=1}^{Z^i-1} |r_k^i|, \tag{1}$$

where  $r_k^i (= \mathbf{R}_{k+1}^i - \mathbf{R}_k^i)$  is the bond vector of the adjacent two  $(k, k + 1)$  slip-links. The stretch ratio  $\lambda^i$  is defined as

$L^i/L_{eq}^i$ , where  $L_{eq}^i (= aZ_{eq}^i)$  is the equilibrium length of  $L^i$ .

This model contains the three relaxation mechanisms considered in the recent tube model (Larson 1999): reptation, contour length fluctuation (CLF), and constraint release (CR). It is assumed that the tension on a chain is always balanced within time  $\tau_e$ . Note that the major difference between the DT model and the PCN model is the nonexistence of the dynamics originating from the tensile balance. Therefore, the momentum equation of the slip-link contains only affine deformation as

$$\frac{d\mathbf{R}_k^i}{dt} = \boldsymbol{\kappa} \cdot \mathbf{R}_k^i, \tag{2}$$

where  $\boldsymbol{\kappa} = (\nabla \mathbf{v})^T$ , i.e.,  $\kappa_{\alpha\beta} = \nabla_\beta v_\alpha$  is the velocity gradient. The primitive path length  $L^i(t)$  follows the overdamped Langevin equation with the Rouse relaxation time of a chain  $\tau_R^i = \tau_e(Z_{eq}^i)^2$ ,

$$\frac{dL^i}{dt} = -\frac{f^i}{\tau_R^i}(L^i - L_{eq}^i) + \left(\frac{dL^i}{dt}\right)_{affine} + \sqrt{\frac{2a^2}{3\tau_e Z_{eq}^i}} w_{clf}(t), \tag{3}$$

where  $f^i (\equiv \{1 - (1/\lambda_{max}^i)^2\} / \{1 - (\lambda^i/\lambda_{max}^i)^2\})$  is the FENE parameter of the  $i$ th chain, and  $\lambda_{max}^i$  is the maximum stretch ratio of the  $i$ th chain.  $w_{clf}(t)$  is a Gaussian white noise satisfying these relations:

$$\langle w_{clf}(t) \rangle = 0, \quad \langle w_{clf}(t) w_{clf}(t') \rangle = \delta(t - t'). \tag{4}$$

The three terms of the RHS in Eq. 3 refer to the contributions of the chain length restoration, the affine deformation, and the contour length fluctuation by thermal noise. By assuming a tension balance along strands, the two tails take over the change of  $L$  half by half on behalf of the pinned slip-links. Thus, the lengths of the two ends  $s_{head}^i$  and  $s_{tail}^i$  change according to the following equations:

$$\begin{aligned} \frac{ds_{head}^i}{dt} &= \frac{1}{2} \left( \frac{dL^i}{dt} - \left(\frac{dL^i}{dt}\right)_{affine} \right) + \sqrt{2D_c^i} w_{rep}(t), \\ \frac{ds_{tail}^i}{dt} &= \frac{1}{2} \left( \frac{dL^i}{dt} - \left(\frac{dL^i}{dt}\right)_{affine} \right) - \sqrt{2D_c^i} w_{rep}(t), \end{aligned} \tag{5}$$

where  $D_c^i (= (L_{eq}^i)^2 / \pi^2 \tau_{rep}^i)$  is the diffusion constant of pure reptation motion and  $\tau_{rep}^i = 3(Z_{eq}^i)^3 \tau_e$  is the reptation time calculated from the Doi-Edwards model (Doi and Edwards 1986). The first term in the RHS in Eq. 5 is related to the contributions in Eq. 3 except for the affine deformation, and the second term is related to the thermal fluctuations. Here,  $w_{rep}(t)$  is a Gaussian white noise that satisfies the same equation as Eq. 4 of  $w_{clf}$ . The lengths of the two ends are checked every  $\tau_e$ . If the length of an end is more than  $a$  or less than zero, the creation or annihilation of

entanglement occurs, respectively, which mimics constraint renewal.

The stress  $\sigma$  of the system consisting of  $N_{\text{chain}}$ -chains in the volume  $V$  is calculated with the Kramers formula:

$$\sigma = \sigma_e \left\langle f \frac{\mathbf{r}\mathbf{r}}{a|\mathbf{r}|} \right\rangle. \quad (6)$$

The unit stress  $\sigma_e$  is related to the plateau modulus  $G_N$  as

$$\sigma_e = \frac{3k_B T}{V} \sum_{i=1}^{N_{\text{chain}}} Z_{\text{eq}}^i = \frac{3\rho RT}{M_e} = \frac{15}{4} G_N, \quad (7)$$

where  $\rho$  is the mass density,  $R$  is the gas constant,  $k_B$  is the Boltzmann constant,  $T$  is the temperature, and  $M_e$  is the entanglement molecular weight. The plateau modulus  $G_N$  is generally expressed as

$$G_N = A \frac{\rho RT}{M_e}, \quad (8)$$

where the constant  $A$  equals 4/5 when considering the thermal fluctuations of the length along the primitive path (Doi and Edwards 1986). Note that Uneyama and Masubuchi (2021) reported a more detailed analysis of this factor  $A$ .

### SORF expression

At present, the contributions of SORF are determined by empirical order parameters correlated to the stretch and orientation (Yaoita et al. 2012; Costanzo et al. 2016). In this study, we utilize the relation proposed by Yaoita et al. (2012). The expression is accurate enough to reproduce the rheological properties.

We briefly explain the SORF mechanism considered in the original study for a monodisperse polymer melt. To express the segments' orientation and stretch to the elongational direction, Yaoita et al. (2012) proposed the stretch/orientation order parameter  $F_{s/o}$  defined as

$$F_{s/o} \equiv \tilde{\lambda}^2 \bar{S}, \quad (9)$$

where  $\tilde{\lambda} = \lambda/\lambda_{\text{max}}$  and  $\bar{S}$  is the averaged orientation anisotropy, defined as

$$\bar{S}(\mathbf{S}) \equiv |s_1 - s_2|, \quad (10)$$

where  $\mathbf{S} = \langle \mathbf{u}\mathbf{u} \rangle$  is the orientation tensor,  $\mathbf{u} (= \mathbf{r}/|\mathbf{r}|)$  is the normalized bond vector between the adjacent slip-links, and  $s_1$  and  $s_2$  are respectively the maximum and minimum eigenvalues of the orientation tensor.

Yaoita et al. (2012) derived the empirical relation between the friction coefficient  $\zeta$  and the order parameter  $F_{s/o}$ ,

$$\begin{aligned} \frac{\tau_e(F_{s/o})}{\tau_e(0)} &= \frac{\zeta(F_{s/o})}{\zeta(0)} \frac{1}{f_{\text{FENE}}} \\ &= \frac{1}{(1+\beta)^\gamma} \left[ \beta + \frac{1 - \tanh\{\alpha(F'_{s/o} - F'^*_{s/o})\}}{2} \right]^\gamma, \end{aligned} \quad (11)$$

where  $f_{\text{FENE}} (\equiv 1/(1 - \tilde{\lambda}^2))$  is the FENE parameter. For  $F'_{s/o} \equiv f_{\text{FENE}} F_{s/o}$ , the parameters  $\alpha = 20$ ,  $\beta = 5.0 \times 10^{-9}$ ,  $\gamma = 0.15$ , and  $F'^*_{s/o} = 0.14$  are obtained from the experiments in monodisperse PS melts.  $F'_{s/o}$  used here is the same as that used in Yaoita et al. (2012). The reason why they introduced  $F'_{s/o}$  is that it is impossible to experimentally separate  $f_{\text{FENE}}$  from  $F_{s/o}$ . In this study, we just follow the way used by Yaoita et al. (2012). Equation 11 expresses the friction change to a lower value by exceeding the threshold parameter of  $F'_{s/o}$ , and was used for the multichain slip-link model (Masubuchi et al. 2001) and the DT model (Doi and Takimoto 2003). Masubuchi et al. (2014a) used Eq. 11 with the above parameter values to examine polyisoprene and poly(n-butyl acrylate) melts and found that the predictions were improved. Nevertheless, the parameter could not be applied universally for chemical structures; thus, Sato and Taniguchi (2019) reported that a smaller value of  $F'^*_{s/o} \simeq 0.007$  gives better predictions for PI melts.

Note that there are other expressions for SORF. For example, Costanzo et al. (2016) used a power-law-type function to describe friction reduction. While these can also reasonably improve the predictions for the entangled and unentangled polymer melts, the functional form and the order parameter have not yet been fully established.

We also note that the strength of the thermal fluctuation is determined using the friction coefficient under flows through the fluctuation-dissipation theorem. Recently, Watanabe and coworkers discussed the change in the Brownian force intensity under strong flow for unentangled chains (Watanabe et al. 2020, 2021; Sato et al. 2021). Using the modified Rouse (or dumbbell) model to allow the spring strength, friction coefficient, and the strength of the Brownian force to be changed, they formulated rheological quantities under shear and elongational flow. Using these rheological quantities, they found that the fluctuation-dissipation theorem might not be valid under strong flow. Since the origin of the friction is local dynamics, this argument can also be applied to entangled melts. Nevertheless, considering the strength of the thermal fluctuation is outside this study's scope and deferred to future research.

The application of Eq. 11 to the polydisperse melts has arbitrariness in terms of averaging the stretch and the orientational anisotropy. The SORF expressions are thus far obtained from monodisperse polymer melt systems. Unlike a monodisperse system where the state of a chain is statistically the same as the states of the surrounding chains, in a polydisperse system, the state of a component often differs from those of other components. For example, in a bidisperse system, the state of a longer or shorter entangled chain and the state of the environment defined by an average over the surrounding polymer chains might be different under a flow because the two types of chains have different relaxation times. The friction of a chain moving

relative to the surrounding chains can be considered to be a consequence of many-body interaction among them, and the coupling of the state of the entangled chain itself with the environment has not yet been clarified. Therefore, the following question arises regarding how the friction coefficient (in general, friction coefficient tensor) of a polymer chain along its contour is determined by (i) the state of the considering chain and/or (ii) the state of the environment around it, and furthermore, which factor of the two is more dominant, (i) or (ii).

In this study, we investigate bidisperse blend systems composed of long and short chains (hereafter C stands for a component, i.e., C=“short” or “long”), where we consider different types of SORF expressions by replacing the statistical quantities in  $F'_{s/o}$  in Eq. 11. Eight types of SORF expressions for a chain belonging to a component C are possible by changing the averages for the statistical quantities: the chain stretch ratio  $\lambda$  and orientation tensor  $\mathbf{S}$  used in the parameter  $F'_{s/o}$ , i.e.,

$$F'_{s/o}{}^{(X.Y.Z)} = f_{\text{FENE}}(\langle \tilde{\lambda} \rangle_X) F_{s/o}(\langle \tilde{\lambda} \rangle_Y, \mathbf{S}_Z), \quad (12)$$

for the bidisperse blend systems instead of  $F'_{s/o}$  in Eq. 11. The superscript X.Y.Z refers to averaging the arguments, where X stands for the normalized stretch ratio in the FENE factor, Y for the normalized stretch ratio in the order parameter  $F_{s/o}$ , and Z for the orientation.  $F'_{s/o}$  consists of the two contributions  $f_{\text{FENE}}$  and  $F_{s/o}$ , and one can consider that two contributions may have different physical origins. For instance, in a monodisperse polymer system, the average quantities used in the two contributions are considered to be identical; in a bidispersed polymer system, they might be different because the state of a considering type of chain, e.g., a long chain can be different from the average over the whole long and short chains. Therefore, we retain possible combinations of variables in  $F'_{s/o}$  and discuss later which combination is the better one.

The component average of a quantity  $Q$ ,  $\langle Q \rangle_C$  means the average of  $Q$  over the chains with the same equilibrium length as a considering chain; on the other hand, the system average of  $Q$ ,  $\langle Q \rangle_S$  expresses overall average of the chains (in other words, environment around the considering chain). The subscripts S and C indicate the averages of stretch and orientation over the system and the component, respectively. For example, the superscript C.S.S on  $F'_{s/o}$  means the component average is used for the FENE parameter, the system average for the stretch ratio  $\lambda$ , and the orientation tensor  $\mathbf{S}$  in  $F_{s/o}$ . Note that Takeda et al. (2015) used the system averages for all quantities in  $F'_{s/o}$ ; specifically, they used  $F'_{s/o}$ , expressed as S.S.S in our notation.

In the next section, we focus on the three combinations, i.e., C.S.S, C.C.S, and S.S.S. Here, we can consider the eight combinations at maximum. However, the four combinations S.S.Z and X.C.C clearly give no meaningful

results in agreement. In the remaining half, the two expressions, C.S.S and S.C.S, gave similar results to each other for the examined samples in this study. Considering the roles of the factors in  $F'_{s/o}$ , the factor  $f_{\text{FENE}}$  comes from the finite extensibility of chains, so we consider it natural that  $f_{\text{FENE}}$  is reflected from the state of the considered chain. In the next section, we discuss the results using C for X in X.Y.Z on supposing the factor  $f_{\text{FENE}}$  reflects the finite extensibility of the chains under consideration. The remaining two combinations, C.C.S and C.S.C, provide mutually similar results to each other for the examined samples. C.C.S clearly focuses on the stretch ratios of the considered chains and the orientation anisotropy of the entire system. On the other hand, the interpretation of C.S.C on the physical meanings has considerable complexity. Therefore, we provide the results in C.C.S, and the discussion on the difference between C.C.S and C.S.C is excluded from the target of this research. To summarize, in the next section, we discuss the results for three cases: S.S.S, C.S.S, and C.C.S; i.e., S.S.S is chosen as a reference case for the previous research where just system averages were used, and C.S.S and C.C.S are chosen as the representative cases where the component average for the stretch of the considered chains is taken into account.

## Results and discussion

The systems considered here are bidisperse polymer blends. In Table 1, we show the characteristics of each system and their simulation conditions. The sample code is given as PS-AAAS-BBBL-CCw, where PS (or PI) stands for polystyrene (or polyisoprene), AAA is the molecular weight of the main-polymer component in the unit of kDa, BBB also denotes the molecular weight of the secondary polymer component in the unit of kDa, and CC expresses the weight percent of the secondary component in the system.  $Z^S$  is the number of entanglements at equilibrium  $Z_{\text{eq}}$  for the short chain (the main component), and  $Z^L$  denotes that for the long chain (the secondary component).

We first compare the storage modulus  $G'(\omega)$  and the loss modulus  $G''(\omega)$  calculated from the simulations with experimental results to determine the unit values  $\tau_e$  and  $\sigma_e$ , and thus obtain the Rouse relaxation time  $\tau_R (= Z_{\text{eq}}^2 \tau_e)$  and the longest relaxation time  $\tau_d$ . The fitted parameters are  $\tau_e = 0.16$  s and  $\sigma_e = 0.68$  MPa for 130 °C PS melts. These values are of similar order to the previous reports by Masubuchi and Amamoto (2016) and Sato and Taniguchi (2019). For 25 °C PI melts, the values are  $\tau_e = 1.1 \times 10^{-5}$  s and  $\sigma_e = 1.2$  MPa. In Appendix, we show the fitted complex moduli for the bidisperse PS and PI melts and the monodisperse PS melts containing polymers of the same molecular weight polymers as before blending,

**Table 1** Conditions with experiments and simulations

No.	Sample code	$Z^S$	$Z^L$	$\lambda_{\max}$	$T$ [°C]	$\tau_e$ [s]	$\sigma_e$ (MPa)
I	PS-.95S-545L-50w	8.6	50	4.4	130	0.16	0.68
II	PS-.52S-390L-.4w	4.5	36	4.4	130	0.16	0.68
III	PS-.52S-390L-14w	4.5	36	4.4	130	0.16	0.68
IV	PS-100S-390L-14w	9.1	36	4.4	130	0.16	0.68
V	PI-.23S-226L-20w	5.3	53	5.9	25	$1.1 \times 10^{-5}$	1.2
VI	PI-.23S-226L-40w	5.3	53	5.9	25	$1.1 \times 10^{-5}$	1.2

as shown in Figs. 5, 6, 7, and 8. The predictions of the linear viscoelasticities (LVEs) are in agreement with the experimental results obtained from the blends.

### Comparison of the different SORFs

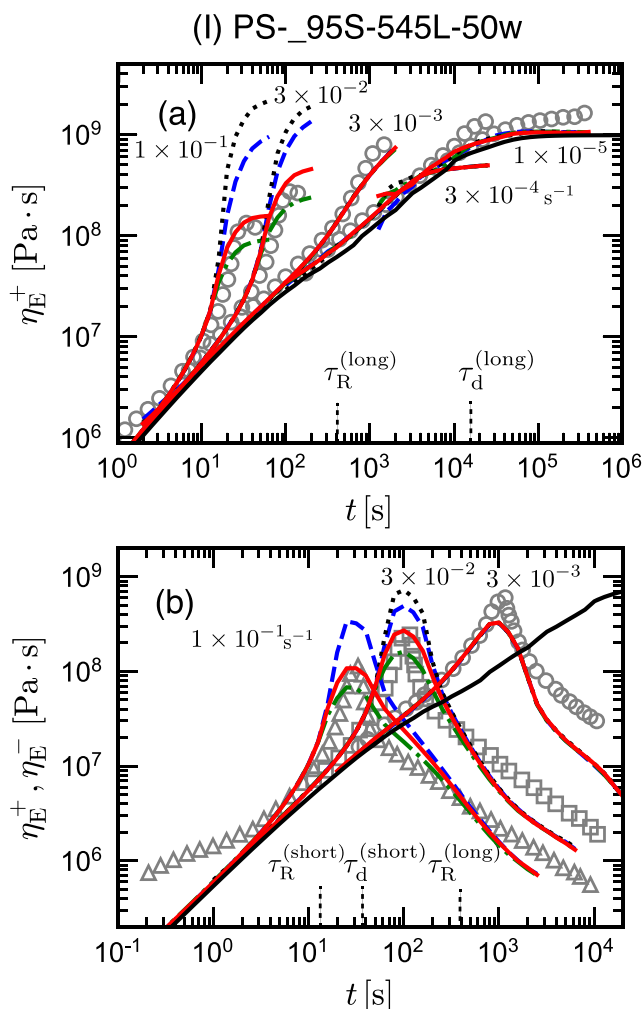
In this section, we compare selected SORF expressions defined in Eq. 12 to the experimental results for the uniaxial elongations. Figures 1 and 2 show the predictions with the extended DT model for the transient viscosities under elongational flows. Figure 1 displays the stress growth and relaxation for the bidisperse system-I reported by Hengeller et al. (2016), which consists of the high weight fraction of the long chains (50 wt%). In contrast, Fig. 2 expresses the transient viscosities of the three samples with low weight fractions (4–14 wt%). The two out of the three samples, II and IV, are reported by Nielsen et al. (2006) and III is reported by van Ruymbeke et al. (2010).

Figure 1 shows (a) elongational transient viscosities and (b) transient viscosities ( $\eta_E^+$  for the start-up and  $\eta_E^-$  after the cessation) in stress-growth-and-relaxation measurements of (I) PS-.95S-545L-50w under elongational flows. In Fig. 1a, the five series data points of the transient viscosities expressed as the symbols are for the experiments with constant elongational strain rates:  $1 \times 10^{-5}$ ,  $3 \times 10^{-4}$ ,  $3 \times 10^{-3}$ ,  $3 \times 10^{-2}$ , and  $1 \times 10^{-1} \text{ s}^{-1}$  from right to left. Figure 1b shows the three data points of the stress growth and relaxation after the cessation, displaying initial uniaxial elongation deformation with a constant strain rate up to the fixed Hencky strain  $\varepsilon_0 = 3.5$  and then a strain rate set to zero. The three strain rates are  $3 \times 10^{-3}$ ,  $3 \times 10^{-2}$ , and  $1 \times 10^{-1} \text{ s}^{-1}$ . As a reference, the Rouse relaxation time and the longest relaxation time are evaluated to be  $\tau_R^{(\text{long})} (= (Z^L)^2 \tau_e) = 4.0 \times 10^2 \text{ s}$  and  $\tau_d^{(\text{long})} = 1.6 \times 10^4 \text{ s}$  for the long chain, respectively. The relaxation times of the short chains are smaller than those of the long chains, which are  $\tau_R^{(\text{short})} (= (Z^S)^2 \tau_e) = 12 \text{ s}$  and  $\tau_d^{(\text{short})} = 36 \text{ s}$ . These quantities for this sample I and those for other samples (II–IV) and appear later as obtained by the analyses of the linear viscoelasticity data (see Appendix).

In Fig. 1a and b, the predictions by extended DT models with C.S.S (colored solid lines), C.C.S (colored dash-dotted lines), S.S.S (colored dashed lines), and by the DT model without SORF (black dotted lines) are shown. From these figures, both C.S.S and C.C.S are in agreement with the experimental results. On the other hand, those for S.S.S (colored dashed lines) and without SORF overestimate the experimental values in the two high-deformation-rate flows:  $3 \times 10^{-2}$ , and  $1 \times 10^{-1} \text{ s}^{-1}$ , which are in the region  $\dot{\varepsilon} > 1/\tau_R^{(\text{long})}$ . When comparing the predictions with C.S.S and C.C.S, C.S.S gives the best prediction for the steady values of the transient viscosities and the maximum values for the stress growth. Under flows, the averaged stretch has the relation:  $\langle \lambda \rangle_{C=\text{“long”}} > \langle \lambda \rangle_S > \langle \lambda \rangle_{C=\text{“short”}}$ . Thus, the contribution of SORF is larger when using C.S.S and C.C.S, that is, the notable failure of S.S.S for  $\dot{\varepsilon} > 1/\tau_R^{(\text{long})}$  comes from the less effect of SORF on the stress. Regarding the average of  $\lambda$  used in  $f_{\text{FENE}}$ , the results obtained by the component average is better than those by the system average. Thus,  $f_{\text{FENE}}$  in  $F'_{s/o}$  should be determined by the average over the chains of the same type as the considering chain as expected in section “SORF expression.”

In Fig. 1a, the nonlinear behavior of the DT model changes from strain softening to strain hardening with increasing the elongational strain rate. However, the experimental results of (I) PS-.95S-545L-50w do not show such strain softening of the simulation results for the middle elongational strain rate region  $1/\tau_R^{(\text{long})} < \dot{\varepsilon} < 1/\tau_d^{(\text{long})}$ . We suppose that the relaxation of the long chain is overestimated compared to that expected from the experiments for bidisperse blend systems. The underestimation of the transient viscosities appears in previous studies for polydisperse polymer melts with the original Doi-Takimoto model (Doi and Takimoto 2003) and for bidisperse polymer melts with the multichain slip-link model (Takeda et al. 2015).

In Fig. 1b, especially in the case of  $\dot{\varepsilon} = 1.0 \times 10^{-1} \text{ s}^{-1}$ , the best prediction by C.S.S (green solid line) cannot fully reproduce the two-step relaxation after flow cessation. Considering the time, the first of the two-step



**Fig. 1** (a) Elongational transient viscosities and (b) transient viscosities in stress-growth-and-relaxation measurements of (I) PS-95S-545L-50w reported by Hengeller et al. (2016), showing initial uniaxial elongation deformation with a constant elongational strain rate up to the fixed Hencky strain  $\epsilon_0 = 3.5$  and then a strain rate set to zero. The colored lines and black dotted lines are the results obtained by the extended DT model with and without SORF, respectively. The blue dashed, red solid, and green dash-dotted lines correspond to the SORFs calculated from the different combinations for X\_Y\_Z: S\_S\_S, C\_S\_S, and C\_C\_S, respectively. The black solid line indicates the LVE result. (a) The circles are the experimental results under elongational flows having the five strain rates:  $1 \times 10^{-5}$ ,  $3 \times 10^{-4}$ ,  $3 \times 10^{-3}$ ,  $3 \times 10^{-2}$ , and  $1 \times 10^{-1} \text{ s}^{-1}$  from right to left. (b) The circles, squares, and triangles represent the experiments with the three respective elongational strain rates  $3 \times 10^{-3}$ ,  $3 \times 10^{-2}$ , and  $1 \times 10^{-1} \text{ s}^{-1}$  from right to left

relaxation behavior seems to correspond to the Rouse relaxation time of the short chains. It is assumed that the fast dynamics of the tensile balance not considered here cause the deviation. In the long-term regime, the predictions show underestimates of the elongational viscosity from the experimental results after cessation, notably for the lower deformation rates. Sato and Taniguchi (2019) demonstrate

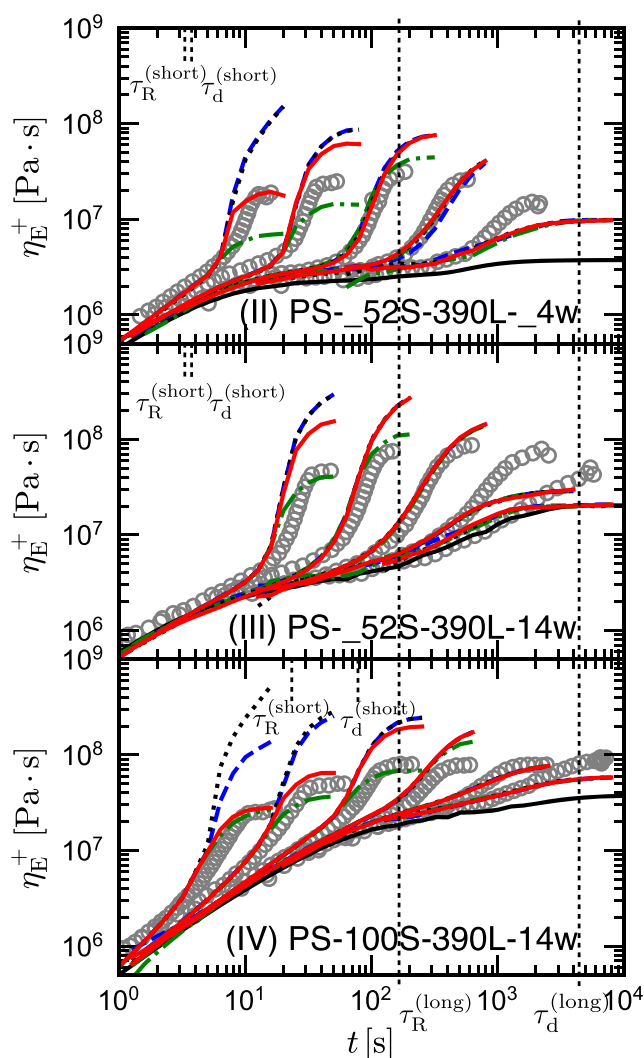


**Fig. 2** Transient elongational viscosities of (II) PS-52S-390L-4w, (III) PS-52S-390L-14w, and (IV) PS-100S-390L-14w. (circles) The data in graphs II and IV are obtained from Nielsen et al. (2006), and the data in graph III are obtained from van Ruymbek et al. (2010). The blue dashed, red solid, and green dash-dotted lines correspond to the SORFs calculated from the different arguments: S\_S\_S, C\_S\_S, and C\_C\_S, respectively. The black dotted and solid lines are the simulation results without the SORF and the LVE result, respectively. The vertical lines across the graphs correspond to the Rouse and longest relaxation times of the long chain. The circles are the experimental results under elongational flows having six strain rates:  $1 \times 10^{-3}$ ,  $3 \times 10^{-3}$ ,  $1 \times 10^{-2}$ ,  $3 \times 10^{-2}$ ,  $1 \times 10^{-1}$ , and  $3 \times 10^{-1} \text{ s}^{-1}$  from right to left. Here, the graphs for II, III, and IV show the experimental results with only the five smaller strain rates, only the five larger strain rates, and all the strain rates, respectively

the predictions for PS145k show the deviation similar to this at the long time region. We consider that the dynamics of the long chains dominate the relaxation on the long time scale, but the relaxation of the long chains in our model seems faster than that expected by the experimental results.

Through these results for (I) PS-95S-545L-50w in Fig. 1, we find that the statistical averages over each

component are important in the system with the high weight fraction (50wt%) of the long chains, where C.S.S is the best one. The success of C.S.S, as well as C.C.S, implies that  $f_{\text{FENE}}$  should be evaluated from the considering chains. In system (I), dominated by the long chains of 50 wt%, the system averages used to evaluate  $F_{s/o}$  reasonably match the component averages over the long chains. Hence, the difference in  $F'_{s/o}$  between C.S.S and C.C.S should be small. In the next paragraph, by using the three types of expressions of  $F'_{s/o}$ , we discuss the prediction of rheology for the systems with the lower-weight fractions of the long chains.

Figure 2 displays the transient elongational viscosities  $\eta_E^+$  for (II) PS-52S-390L-4w, (III) PS-52S-390L-14w, and (IV) PS-100S-390L-14w. The data in graphs II and IV are obtained from Nielsen et al. (2006), and the data in graph III are obtained from van Ruymbeke et al. (2010). The characteristic times of the long chain have the values  $\tau_R^{(\text{long})} = 2.1 \times 10^2$  s and  $\tau_d^{(\text{long})} = 5.0 \times 10^3$  s for PS390k. The values of the short chain for II and III are  $\tau_R^{(\text{short})} = 3.2$  s and  $\tau_d^{(\text{short})} = 3.8$  s for PS52k, and those for IV are  $\tau_R^{(\text{short})} = 13$  s and  $\tau_d^{(\text{short})} = 44$  s for PS100k. The circles are the experimental results under elongational flows having the five elongational strain rates  $3 \times 10^{-3}$ ,  $1 \times 10^{-2}$ ,  $3 \times 10^{-2}$ ,  $1 \times 10^{-1}$ ,  $3 \times 10^{-1}$  s $^{-1}$  for II and under the elongational flows also having the five elongational strain rates:  $1 \times 10^{-3}$ ,  $3 \times 10^{-3}$ ,  $1 \times 10^{-2}$ ,  $3 \times 10^{-2}$ , and  $1 \times 10^{-1}$  s $^{-1}$  for III from right to left. For IV, the elongational flows have the six elongational strain rates  $1 \times 10^{-4}$ ,  $3 \times 10^{-3}$ ,  $1 \times 10^{-2}$ ,  $3 \times 10^{-2}$ ,  $1 \times 10^{-1}$ , and  $3 \times 10^{-1}$  s $^{-1}$ . In the three figures for II (top), III (middle), and IV (bottom), the SORF effects with the component averages (C.S.S and C.C.S) fundamentally improve the predictions for the higher elongational strain rates than  $1/\tau_R^{(\text{long})}$ , which correspond to the two or three  $\dot{\epsilon}$  cases from the left. On the other hand, the predictions with the SORF effects just with the system averages (S.S.S expressed by colored dashed lines) are almost the same as those without SORF, especially in the results of II and III. The predictions of C.S.S (colored solid lines) are the best for sample II, those of C.C.S (colored dash-dotted lines) are the best for sample III, and those of C.S.S and C.C.S are in agreement for sample IV.

By focusing on the data from the higher deformation-rate flows ( $\dot{\epsilon} > 1/\tau_R^{(\text{long})}$ ), we find that the C.S.S and C.C.S predictions are the best for the steady viscosities in the two results, II and III, respectively. The SORF expression with C.C.S shows the best results for the two samples, (III) PS-52S-390L-14w and (IV) PS-100S-390L-14w, while the predictions underestimate the viscosities for the two samples (I) PS-95S-545L-50w and (II) PS-52S-390L-4w. On the other hand, the predictions obtained from C.S.S are the best for the two samples, I and

II. The two samples, I and II, have the long chain's high and low weight fractions (50wt% and 4wt%) and are dominated by the contributions of the long and short chains, respectively. Thus, on the assumption that the order parameter  $F_{s/o}$  should describe the environment around the considered chain in the experiments, we find that the  $F_{s/o}$  obtained from the system averages rather than the component averages can describe the elongational rheological properties of the two systems, I and II. On the other hand, this  $F_{s/o}$  obtained from the system averages does not fully describe the two systems, III and IV, with the long chain's middle weight fractions.

In this section, we found that the importance in using the component averages from the comparison in the different SORFs. The SORF expression with the component average improves the predictions for all the examined samples having the molecular weights (4–50 wt%) of the minor component under the high-deformation-rate flows with a large elongational strain rate ( $\dot{\epsilon} > 1/\tau_R^{(\text{long})}$ ). For the dynamics of the polymer chain, taking into account the state of the considered chain is necessary for the evaluation of the reduction of friction. We should confirm how much the condition of a shorter or longer component is extremely different from that of the other under flows. In the next subsection, we investigate how much difference in the states appears between long and short chains.

## Further applications

Next, we investigate the rheological properties of bidisperse blend systems and the state for each component of polymer chains by using the DT model with a SORF expression using the component averages (C.S.S as an example). As shown in the previous section, we could not find the clear superiority or inferiority between C.S.S and C.C.S; of course, these two are superior to the other combination, say, S.S.S. The expressions S.Y.Z and C.C.C do not take this aspect into consideration because they do not give better results or it is difficult to give clear physical meanings to them. For example, it has been confirmed that the results with C.C.C show a clear underestimate for the experimental results although we do not show data in the present paper due to excessively large deviations.

Thus, the reason to use C.S.S and not C.C.S is the simplicity and relatively clear physical meaning of the formula, in that the FENE parameter  $f_{\text{FENE}}$  in Eq. 11 expresses the contribution of the considered chains and the order parameter  $F_{s/o}$  in Eq. 11 expresses that from the environment. Figure 3 displays the steady-state properties for the three PS samples reported by Nielsen et al. (2006) for investigating the difference in the states of the long and short chains under elongational flows. In addition, to test the chemical dependence of the friction reduction mechanism in



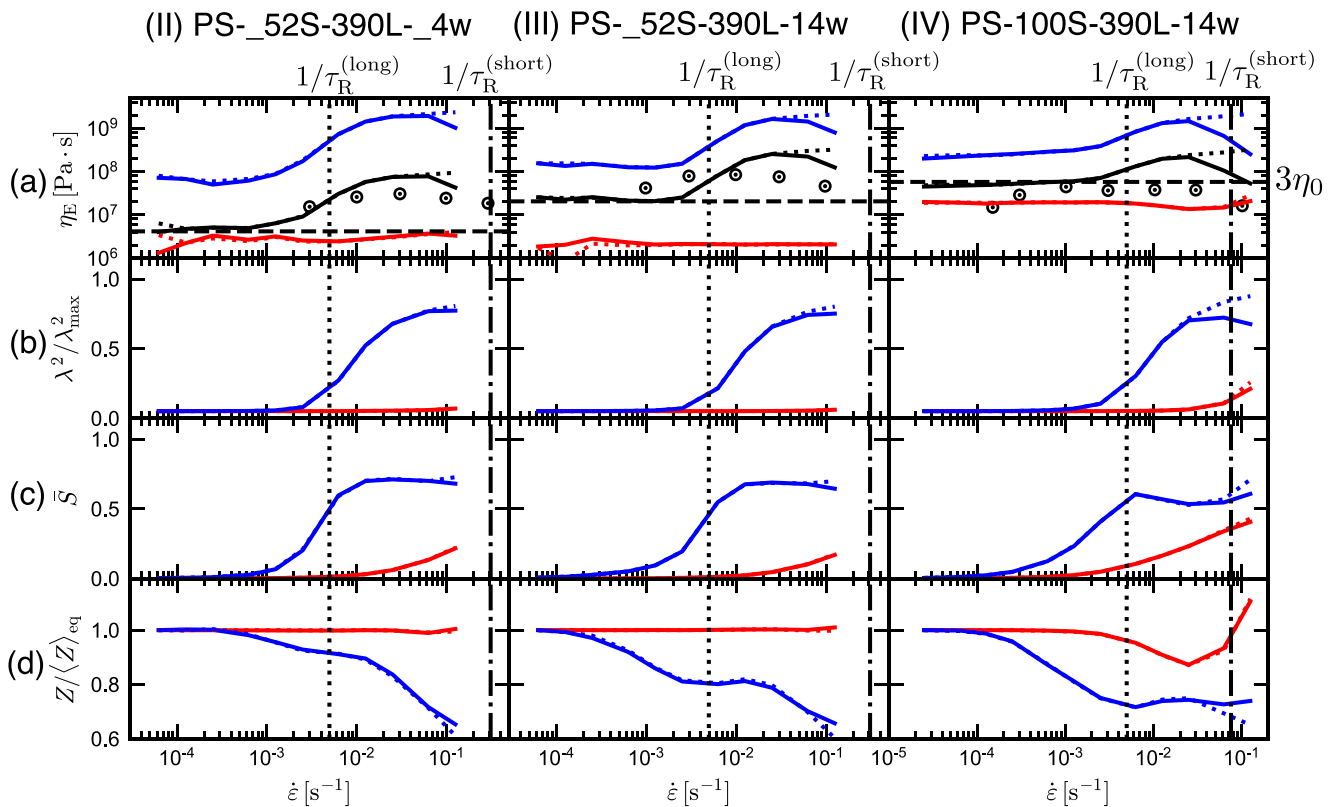


**Fig. 3** (a) Elongational viscosities, (b) normalized stretch rates, (c) orientational anisotropy, and (d) normalized numbers of entanglements for (II) PS-52S-390L-4w, (III) PS-52S-390L-14w, and (IV) PS-100S-390L-14w. The black, red, and blue lines with symbols express the statistical value averaged over the system, the major component (short chains), and the minor component (long chains),

respectively. The solid and dotted lines correspond to the results with and without the SORF mechanism, respectively. In graph (a), the dashed horizontal line displays the three times of the zero viscosity  $3\eta_0$  calculated from the LVE results by the DT model, and the dotted and dash-dotted vertical lines show the inverse of the Rouse relaxation times  $\tau_R$  of the long and short chains

other bidisperse polymer melts, we also study the transient viscosities under steady shears in Fig. 4 with two PI systems reported by Read et al. (2012).

Figure 3 shows the (a) steady state elongation viscosity, (b) stretch ratio, (c) orientation anisotropy, and (d) numbers of entanglements on a chain for (II) PS-52S-390L-4w, (III) PS-52S-390L-14w, and (IV) PS-100S-390L-14w, from top to bottom. The solid and dotted lines are the results with and without SORF, respectively. Here, we adopt the  $C_{S,S}$  expression to evaluate the parameter  $F'_{s/o}$ . The red and blue lines are the averages over short chains and long chains, respectively. The black solid lines and the black dashed lines are the steady viscosities and the LVE results, respectively. The symbols are the experimental values having unimodal shapes obtained from the report by Nielsen et al. (2006). As seen from the three columns of II (left), III (center), and IV (right), the states of the short and long chains are notably different from each other. The long chains are fully oriented and stretched under the region where the anisotropy and the stretch of the short chain do not largely change. The

difference in the state between the components should be critical when considering friction reduction.

The decrease in the steady elongation viscosities appears under high-deformation-rate flows, while the orientational anisotropy of the short chains increases. This tendency of the decrease is in agreement with the experimental results. From the right column for IV, the behavior in the steady viscosities clearly appears to suppress the stretch ratios of the long chains. In the left column II, the steady viscosities evaluated by the DT model with and without the SORF are slightly different for the small strain rate region, and the difference is considered to originate from the thermal fluctuations. Note also that the steady viscosities obtained by the PCN model (Takeda et al. 2015) slightly increase even with the small elongational strain rate, but our simulations do not show such increases. The major difference between their PCN model and the DT model is whether the dynamics of the force balances exist. The strands of the long chains pull the short chains, and both dynamics with and without force balance may cause the difference.

In the left and center columns for II and III, the (a) viscosities, (b) stretch ratios, and (c) orientational anisotropy are similar to each other, but (d) the numbers of entanglements of (III) PS-52S-390L-14w remarkably decrease around the vertical dotted line ( $1/\tau_R^{(\text{long})}$ ) with the elongational strain rate compared to those of (II) PS-52S-390L-4w. The difference between II and III systems is simply the weight percent of the minor component (the long chains), that is, the ease in the releasing “long-long” chains entanglements changes more than that in the “long-short” chains entanglements under convection. We suppose that the long chains easily release the entanglements under the small elongational deformation rate flows.

In the right column of Fig. 3d, the normalized number of entanglements shows an upturn in the high deformation rate region. We consider that the upturn of  $\langle Z \rangle / Z_{\text{eq}}$  is unphysical, and should be improved. Nevertheless, the previous study (Sato and Taniguchi 2019) demonstrates that the increase of  $Z$  in the region  $\dot{\epsilon} > 1/\tau_R$  does not bring the unreasonable rheological properties and the unphysical conformation since the increased entanglements near the ends only slightly contributes to the stress. Since the upturn is not observed in the PCN model from the comparison with the DT model reported by Sato and Taniguchi (2019), this might come from the difference between the DT model and the PCN model, e.g., the Rouse dynamics faster than  $1/\tau_R$ .

Figure 4 shows the transient viscosities ( $\eta^+$  for shear and  $\eta_E^+$  for elongation) of (V) PI-23S-226L-20w under steady shears and (VI) PI-23S-226L-40w under steady shears and uniaxial elongations. The values of the two units,  $\tau_e$  and  $\sigma_e$ , are already written in the second paragraph of section “Results and discussion.” The characteristic times of the long chain have the values  $\tau_R^{(\text{long})} = 3.1 \times 10^{-2}$  s and  $\tau_d^{(\text{long})} = 1.3$  s for PI226k. Those of the short chain have the values  $\tau_R^{(\text{short})} = 3.1 \times 10^{-4}$  s and  $\tau_d^{(\text{short})} = 4.6 \times 10^{-4}$  s for PI23k.

In Fig. 4, the transient viscosities under small elongational strain rate flows are in agreement with the LVE result for a long time. On the other hand, under sufficiently high elongational strain rate flows, the responses show nonlinearity, i.e., strain hardening within short times. For both samples under shear flows, the viscosities under higher shear rate flows display stress overshoots and a decrease in the steady values with the shear rate. Regarding the transient shear viscosities, simulations both with and without SORF reasonably reproduce the data of (V) PI-23S-226L-20w and (VI) PI-23S-226L-40w, even if the shear rates are larger than the inverse of the Rouse relaxation time of the long chains ( $\dot{\gamma}\tau_R^{(\text{long})} \sim 20$ ), which is the same tendency observed in the Rolie-double-Poly model (Boudara et al. 2019).

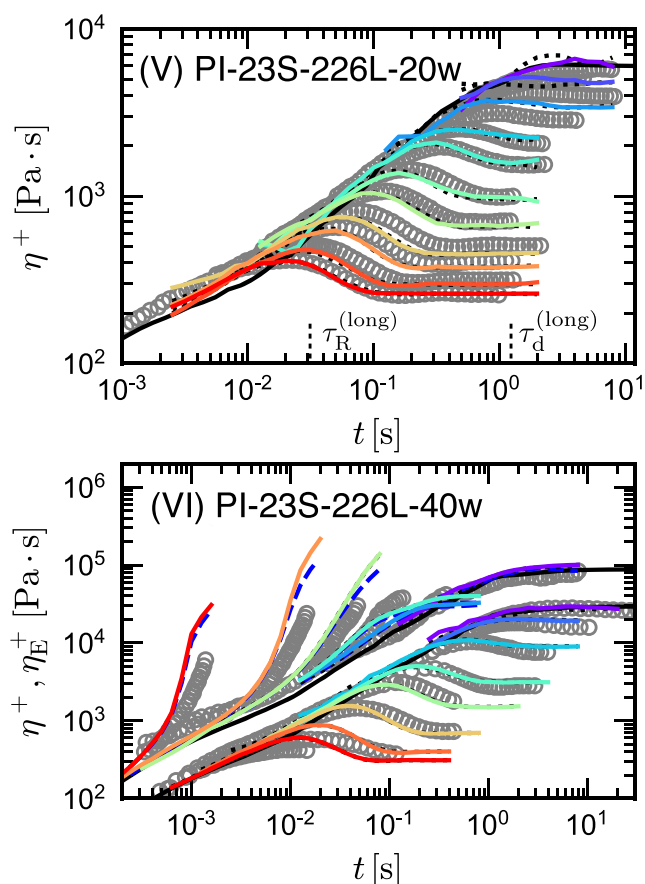


**Fig. 4** The transient viscosities of (V) PI-23S-226L-20w under shear (VI) PI-23S-226L-40w under shear or uniaxial elongation were reported by Read et al. (2012). Colored solid lines and black dotted lines are the results of the extended DT model with or without the SORF, respectively. Blue dashed lines are the results under uniaxial elongations with the tuned parameter  $F_{s/o}^{/*} = 0.007$  by Sato and Taniguchi (2019). The black solid line is the LVE result. Symbols show the experimental results

In the upper part in the graph for VI, the elongational viscosity growth functions are also displayed. The elongational viscosities in the DT model, even with the SORF mechanism, are overestimated compared with the experimental viscosities. Here, remembering that the parameters in Eq. 11 are for polystyrene, Sato and Taniguchi (2019) proposed a different value of the parameter  $F_{s/o}^{/*} = 0.007$  for polyisoprene. With  $F_{s/o}^{/*} = 0.007$ , they have shown that the predictions of the steady viscosities approach the experimental results in the monodispersed polyisoprene. Thus, we test the proposed parameter for the bidispersed polyisoprene melts, expecting the overestimations to be suppressed. The lower graph for (VI) PI-23S-226L-40w shows the elongational viscosities with  $F_{s/o}^{/*} = 0.14$  (black solid lines) and  $F_{s/o}^{/*} = 0.007$  (blue dashed lines). The results with the smaller  $F_{s/o}^{/*} = 0.007$  approach the experimental results

under flows with high elongational strain rates, but still, the  $F'_{s/o} = 0.007$  does not bring sufficiently good agreement to the data of the nonlinear behavior between the simulations and the experiments. Judging from these deviations, the chemical dependence of the friction reduction mechanism and the appropriate functional form and parameters are not resolved in this study and should be sought in a future study.

In this section, we have confirmed the three following findings: (i) The states of the long chain and the short chain clearly differ from each other under steady elongations; (ii) the DT model with SORF using the component average (C.S.S) brings the improvement in the prediction not only for the transient viscosities but also for the steady state elongational viscosities, and (iii) for shear flows, the results with and without SORF predictions are not important for shear flows even with a high shear rate ( $\dot{\gamma} \tau_R^{(\text{long})} \sim 20$ ).

## Conclusions

We studied the rheological predictions by dual slip-link model (extended version of the Doi-Takimoto model) for six samples of the bidisperse entangled polymer melts that have already been measured experimentally. In the extended model, the improvement of stretch- and orientation-induced friction reduction effect is addressed. The rheological predictions basically support the applicability of the SORF expression even for the bidisperse melts under shear and uniaxial elongational flows. The results satisfy the aim of this study: additional confirmation of the SORF mechanism for bidisperse entangled polymer melts.

Through this study, there are three findings. First, the SORF expression proposed by Yaoita et al. (2012) improves the rheological prediction for bidisperse entangled polymer melts under the uniaxial elongational flows with strain rates comparable to or larger than the inverse of the Rouse relaxation time of the longer chain. Second, the predictions with the SORF using the component average for the stretches quantitatively reproduce the steady viscosities because the states of the components with different molecular weights differ from each other under elongational flows. Third, the SORF effect does not affect the prediction of the nonlinear rheology of the bidisperse system under shear even for a high deformation rate for the specific polyisoprene systems. In particular, the second point means that in the frictional dynamics of an entangled polymer chain in a polydisperse system, the state of the considered chain is also important as well as the state of the environment. We show guidelines for the extension of the reduction friction effect obtained from monodisperse melts.

Further studies are clearly required for a deeper understanding of the friction reduction in bidisperse systems. While this study considers two averages (i.e., component and system averages) to reproduce the experimental rheological data, this treatment has not been fully validated. For such a purpose, molecular dynamics simulations are highly desirable.

This study is intended to guide the future application of the SORF expression for the prediction of entangled polymer melts under flows not only with a bidisperse distribution, but also with an arbitrary molecular weight distribution for the analysis of polymer processing. Recently, some multiscale simulation (MSS) studies have focused on this model (Sato and Taniguchi 2017; Sato et al. 2019; Sato and Taniguchi 2021; Hamada et al. 2021) due to the computational convenience. The confirmation of the applicability of the DT model into which the SORF mechanism is incorporated is important for future analysis by using MSS for polymer processing consisting of polydisperse entangled polymer melts. Our research helps better understand effective polymer processing by controlling the molecular weight.

## Appendix. Linear viscoelasticity

The linear relaxation modulus  $G(t)$  is calculated from the autocorrelations as

$$G(t) = \frac{V}{5k_B T} (\langle \sigma_{xy}(t) \sigma_{xy}(0) \rangle + \langle \sigma_{yz}(t) \sigma_{yz}(0) \rangle + \langle \sigma_{zx}(t) \sigma_{zx}(0) \rangle) + \frac{V}{30k_B T} (\langle N_{xy}(t) N_{xy}(0) \rangle + \langle N_{yz}(t) N_{yz}(0) \rangle + \langle N_{zx}(t) N_{zx}(0) \rangle), \quad (13)$$

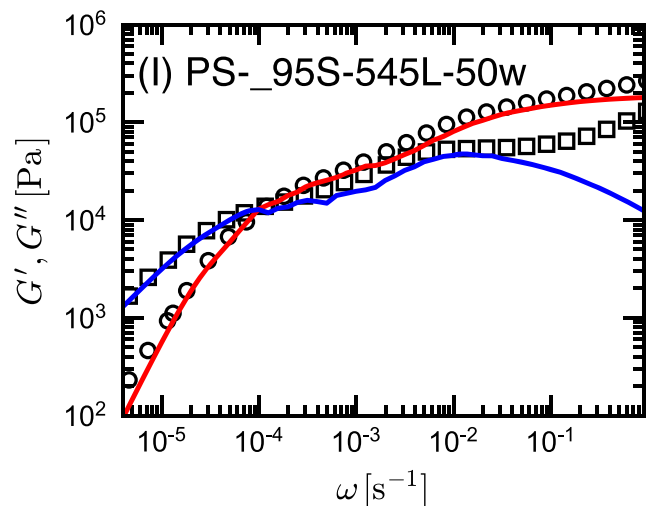


**Fig. 5** Storage (circles and red line) and loss (squares and blue line) moduli of (I) PS-95S-545L-50w. The solid lines represent those obtained by the DT model. Symbols express those obtained by Hengeller et al. (2016)

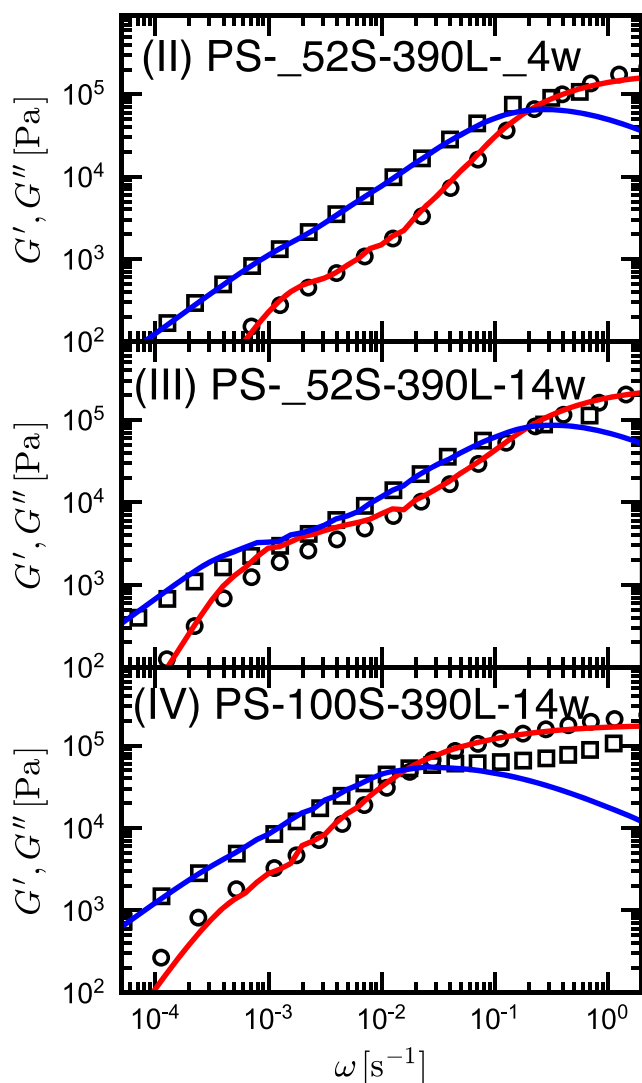


**Fig. 6** Storage (circles and red line) and loss (squares and blue line) moduli of (II) PS-52S-390L-4w, (III) PS-52S-390L-14w, and (IV) PS-100S-390L-14w. The solid lines represent those obtained by the DT model. Symbols express those obtained by Nielsen et al. (2006)

where  $\sigma_{\alpha\beta}$  is the  $\alpha\beta$  component of the stress tensor and  $N_{\alpha\beta}(= \sigma_{\alpha\alpha} - \sigma_{\beta\beta})$  is the normal stress difference. The multiple-tau method (Ramírez et al. 2010) enables us to evaluate the autocorrelations efficiently.

The reference data and the predictions from the extended Doi-Takimoto model are shown by the symbols and black lines, respectively, in Fig. 5 (Hengeller et al. 2016), Fig. 7 (Read et al. 2012), and Fig. 6 (Nielsen et al. 2006). These figures display only the regions of the terminal relaxation and the plateau, which can be calculated by the DT model. The simulation results predict the two contributions of

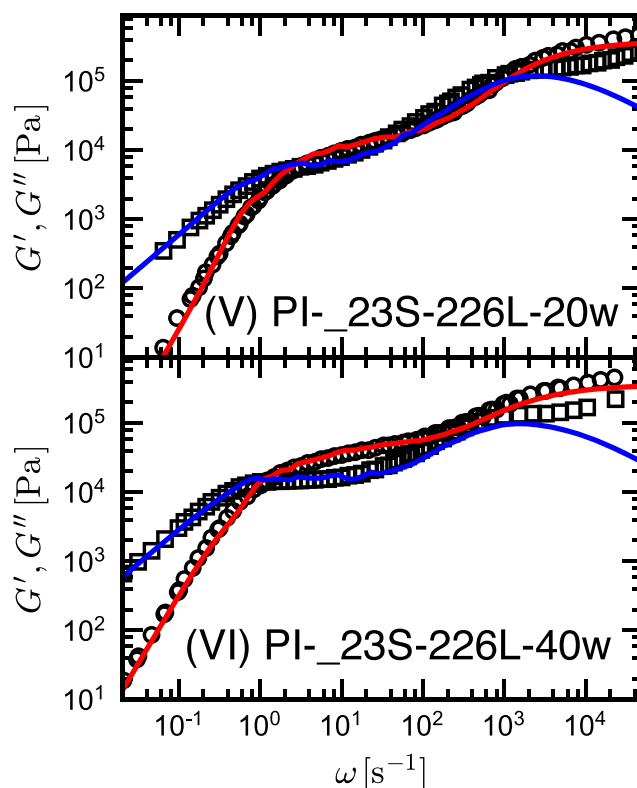


**Fig. 7** Storage (circles and red line) and loss (squares and blue line) moduli of (V) PI-23S-226L-20w, and (VI) PI-23S-226L-40w. The solid lines represent those obtained by the DT model. Symbols express those obtained by Read et al. (2012)

the short chains and the long chains. Figures 5, 6, and 7 show that the DT model can successfully reproduce the linear rheological properties of bidispersed polymers except for the high frequency region. The deviation from the experimental data in the high frequency range is due to the lack of the Rouse-like dynamics in the DT model.

The values of  $\tau_e$  and  $\sigma_e$  are determined from the LVE results of bidisperse entangled polymer melts. Here, we show the comparison between the simulations and the data of monodisperse melts. Figure 8 shows the linear viscoelasticity of the monodispersed polystyrene samples before blended. The numbers of entanglements at equilibrium  $Z_{eq}$  equal 4.5, 8.6, 9.1, 18, 36, and 50 for the molecular weights 52 k, 95 k, 100 k, 200 k, 390 k, and 545 k of the mono-dispersed PS melts (130 °C), respectively. The results from the DT model, the storage and the loss moduli, match almost all the data, but the simulation results for PS95k and PS100k slightly deviate from the data obtained from Hengeller et al. (2016) and Nielsen et al. (2006).

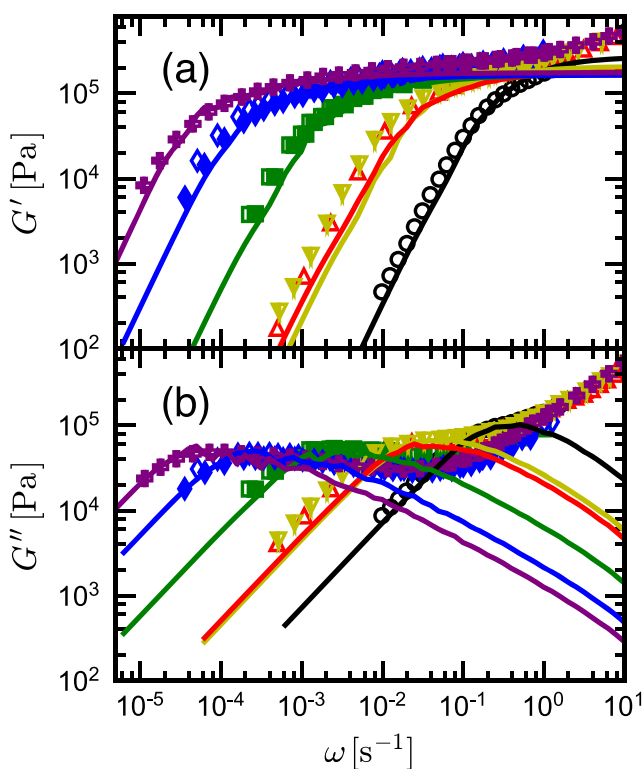


**Fig. 8** (a) Storage modulus and (b) loss modulus. The graphs show the compared results with 130 °C PS52k (Nielsen et al. 2006), PS95k (Hengeller et al. 2016), PS100k (Nielsen et al. 2006), PS200k (Bach et al. 2003; Nielsen et al. 2006), PS390k (Bach et al. 2003; Nielsen et al. 2006), and PS545k (Hengeller et al. 2016). Circles, upper triangles, lower triangles, squares, diamonds, and crosses show the experimental results of PS52k, PS95k, PS100k, PS200k, PS390k, and PS545k, respectively. The unfilled, filled, and left-filled markers show the results of experiments reported by Nielsen et al. (2006), Bach et al. (2003), and Hengeller et al. (2016), respectively. Lines show the results of the DT model simulations

**Acknowledgements** I acknowledge the “Joint Usage/Research Center for Interdisciplinary Large-scale Information Infrastructures” and “High Performance Computing Infrastructure” in Japan (ProjectIDs: jh21001-MDH and jh220054) for supporting and providing computational resources Wisteria/BDEC-01 at the Information Technology Center, University of Tokyo.

**Funding** This work was supported partially by JSPS KAKENHI grant numbers 19H01862 and 21K13893, and by the establishment of university fellowships toward the creation of science technology innovation, grant number JPMJFS2123.

## References

- Bach A, Almdal K, Rasmussen HK, Hassager O (2003) Elongational viscosity of narrow molar mass distribution polystyrene. *Macromolecules* 36:5174–5179. <https://doi.org/10.1021/ma034279q>
- Boudara VAH, Peterson JD, Leal LG, Read DJ (2019) Non-linear rheology of polydisperse blends of entangled linear polymers: Rolie-double-poly models. *J Rheol* 63:71–91. <https://doi.org/10.1122/1.5052320>
- Costanzo S, Huang Q, Ianniruberto G, Marrucci G, Hassager O, Vlassopoulos D (2016) Shear and extensional rheology of polystyrene melts and solutions with the same number of entanglements. *Macromolecules* 49(10):3925–3935. <https://doi.org/10.1021/acs.macromol.6b00409>
- Doi M, Edwards SG (1986) The theory of polymer dynamics. Oxford University Press
- Doi M, Takimoto J (2003) Molecular modelling of entanglement. *Philos Trans R Soc A* 361:641–652. <https://doi.org/10.1098/rsta.2002.1168>
- Ferry JD (1980) Viscoelastic properties of polymers. Wiley
- Hamada Y, Sato T, Taniguchi T (2021) Multiscale simulation of a polymer melt flow between two coaxial cylinders under nonisothermal conditions. *Math Eng* 3:1–22. <https://doi.org/10.3934/mine.2021042>
- Hengeller L, Huang Q, Dorokhin A, Alvarez NJ, Almdal K, Hassager O (2016) Stress relaxation of bi-disperse polystyrene melts: exploring the interactions between long and short chains in non-linear rheology. *Rheol Acta* 55:303–314. <https://doi.org/10.1007/s00397-016-0916-9>
- Hua CC, Schieber JD (1998) Segment connectivity, chain-length breathing, segmental stretch, and constraint release in reptation models. i. theory and single-step strain predictions. *J Chem Phys* 109(22):10:018–10:027. <https://doi.org/10.1063/1.477670>
- Ianniruberto G, Brasiello A, Marrucci G (2012) Simulations of fast shear flows of ps oligomers confirm monomeric friction reduction in fast elongational flows of monodisperse ps melts as indicated by rheo-optical data. *Macromolecules* 45:8058–8066. <https://doi.org/10.1021/ma301368d>
- Ianniruberto G, Marrucci G, Masubuchi Y (2020) Melts of linear polymers in fast flows. *Macromolecules*, 53. <https://doi.org/10.1021/acs.macromol.0c00693>
- Larson RG (1999) The structure and rheology of complex fluids. Oxford University Press, New York
- Likhtman AE (2005) Single-chain slip-link model of entangled polymers: simultaneous description of neutron spin-echo, rheology, and diffusion. *Macromolecules* 38(14):6128–6139. <https://doi.org/10.1021/ma050399h>
- Mantia FPL, Valenza A, Acierno D (1986) Influence of the structure of linear density polyethylene on the rheological and mechanical properties of blends with low density polyethylene. *Eur Polym J* 22:647–652. [https://doi.org/10.1016/0014-3057\(86\)90163-1](https://doi.org/10.1016/0014-3057(86)90163-1)
- Masubuchi Y (2014) Simulating the flow of entangled polymers. *Ann Rev Chem Biomol Eng* 5(1):11–33. <https://doi.org/10.1146/annurev-chembioeng-060713-040401>
- Masubuchi Y, Amamoto Y (2016) Orientational cross-correlation in entangled binary blends in primitive chain network simulations. *Macromolecules* 49:9258–9265. <https://doi.org/10.1021/acs.macromol.6b01642>
- Masubuchi Y, Takimoto JI, Koyama K, Ianniruberto G, Marrucci G, Greco F (2001) Brownian simulations of a network of reptating primitive chains. *J Chem Phys* 115:4387–4394. <https://doi.org/10.1063/1.1389858>
- Masubuchi Y, Matsumiya Y, Watanabe H (2014a) Test of orientation/stretch-induced reduction of friction via primitive chain network simulations for polystyrene, polyisoprene, and poly(n-butyl acrylate). *Macromolecules* 47:6768–6775. <https://doi.org/10.1021/ma5016165>
- Masubuchi Y, Matsumiya Y, Watanabe H, Marrucci G, Ianniruberto G (2014b) Primitive chain network simulations for pom-pom polymers in uniaxial elongational flows. *Macromolecules* 47:3511–3519. <https://doi.org/10.1021/ma500357g>
- Masubuchi Y, Ianniruberto G, Marrucci G (2021) Primitive chain network simulations of entangled melts of symmetric and asymmetric star polymers in uniaxial elongational flows. *J Soc Rheol Jpn* 49:171–178. <https://doi.org/10.1678/rheology.49.171>

- Matsumiya Y, Watanabe H (2021) Non-universal features in uniaxially extensional rheology of linear polymer melts and concentrated solutions. A review. <https://doi.org/10.1016/j.progpolymsci.2020.101325>
- Minegishi A, Nishioka A, Takahashi T, Masubuchi Y, Ji Takimoto, Koyama K (2001) Uniaxial elongational viscosity of ps/a small amount of uhmw-ps blends. *Rheol Acta* 40(4):329–338. <https://doi.org/10.1007/s003970100165>
- Nielsen JK, Rasmussen HK, Hassager O, McKinley GH (2006) Elongational viscosity of monodisperse and bidisperse polystyrene melts. *J Rheol* 50:453–476. <https://doi.org/10.1122/1.2206711>
- Ramirez J, Sukumaran SK, Vorselaars B, Likhtman AE (2010) Efficient on the fly calculation of time correlation functions in computer simulations. *J Chem Phys*, 133. <https://doi.org/10.1063/1.3491098>
- Read DJ, Jagannathan K, Sukumaran SK, Auhl D (2012) A full-chain constitutive model for bidisperse blends of linear polymers. *J Rheol* 56:823–873. <https://doi.org/10.1122/1.4707948>
- Read DJ, Shivokhin ME, Likhtman AE (2018) Contour length fluctuations and constraint release in entangled polymers: slip-spring simulations and their implications for binary blend rheology. *J Rheol* 62:1017–1036. <https://doi.org/10.1122/1.5031072>
- van Ruymbeke E, Nielsen J, Hassager O (2010) Linear and nonlinear viscoelastic properties of bidisperse linear polymers: mixing law and tube pressure effect. *J Rheol* 54:1155–1172. <https://doi.org/10.1122/1.3478316>
- Sato T, Taniguchi T (2017) Multiscale simulations for entangled polymer melt spinning process. *J Non-Newtonian Fluid Mech* 241:34–42. <https://doi.org/10.1016/j.jnnfm.2017.02.001>
- Sato T, Taniguchi T (2019) Rheology and entanglement structure of well-entangled polymer melts: a slip-link simulation study. *Macromolecules* 52:3951–3964. <https://doi.org/10.1021/acs.macromol.9b00314>
- Sato T, Taniguchi T (2021) Multiscale simulation of the flows of a bidisperse entangled polymer melt. *J Soc Rheol Jpn* 49:87–95. <https://doi.org/10.1678/rheology.49.87>
- Sato T, Harada K, Taniguchi T (2019) Multiscale simulations of flows of a well-entangled polymer melt in a contraction-expansion channel. *Macromolecules* 52:547–564. <https://doi.org/10.1021/acs.macromol.8b00649>
- Sato T, Kwon Y, Matsumiya Y, Watanabe H (2021) A constitutive equation for rouse model modified for variations of spring stiffness, bead friction, and brownian force intensity under flow. *Phys Fluid*, 33. <https://doi.org/10.1063/5.0055559>
- Takeda K, Sukumaran SK, Sugimoto M, Koyama K, Masubuchi Y (2015) Primitive chain network simulations for elongational viscosity of bidisperse polystyrene melts. *Adv Model Simul Eng Sci*, 2. <https://doi.org/10.1186/s40323-015-0035-7>
- Takeda K, Masubuchi Y, Kumar SS, Sugimoto M, Koyama K, Masubuchi Y (2018) Re-examination of the effect of the stretch/orientation-induced reduction of friction under equi-biaxial elongational flow via primitive chain network simulation using two definitions of orientation anisotropy. *J Soc Rheol Jpn* 46:145–149. <https://doi.org/10.1678/rheology.46.145>
- Takeda K, Masubuchi Y, Sugimoto M, Koyama K, Sukumaran SK (2020) Simulations of startup planar elongation of an entangled polymer melt. *J Soc Rheol Jpn* 48:43–48. <https://doi.org/10.1678/RHEOLOGY.48.43>
- Uneyama T, Masubuchi Y (2021) Plateau moduli of several single-chain slip-link and slip-spring models. *Macromolecules* 54:1338–1353. <https://doi.org/10.1021/acs.macromol.0c01790>
- Viovy JL, Rubinstein M, Colby RH (1991) Constraint release in polymer melts: tube reorganization versus tube dilation. *Macromolecules* 24(12):3587–3596. <https://doi.org/10.1021/ma00012a020>
- Watanabe H, Matsumiya Y, Sato T (2020) Nonlinear rheology of fene dumbbell with friction-reduction: analysis of brownian force intensity through comparison of extensional and shear viscosities. *J Soc Rheol Jpn* 48:259–269. <https://doi.org/10.1678/rheology.48.259>
- Watanabe H, Matsumiya Y, Sato T (2021) Revisiting nonlinear flow behavior of rouse chain: roles of fene, friction-reduction, and brownian force intensity variation. *Macromolecules* 54(8):3700–3715. <https://doi.org/10.1021/acs.macromol.1c00013>
- Yaoita T, Isaki T, Masubuchi Y, Watanabe H, Ianniruberto G, Marrucci G (2012) Primitive chain network simulation of elongational flows of entangled linear chains: stretch/orientation-induced reduction of monomeric friction. *Macromolecules* 45:2773–2782. <https://doi.org/10.1021/ma202525v>

**Publisher's note** Springer Nature remains neutral with regard to jurisdictional claims in published maps and institutional affiliations.